

1 Theoretical Insights into the Vibrational Structure of Carbon Dioxide 2 Rare-Gas Complexes

3 Larry Rodriguez, Michael Natalizio, and Olaseni Sode*



Cite This: <https://doi.org/10.1021/acs.jpca.4c00639>



Read Online

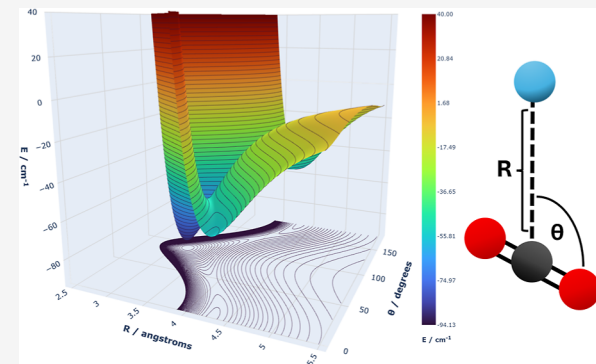
ACCESS |

Metrics & More

Article Recommendations

Supporting Information

4 **ABSTRACT:** Two new flexible-monomer two-body ab initio potential
5 energy surfaces (PESs) for the neon and krypton van der Waals
6 complexes with carbon dioxide were developed extending our previous
7 work on the Ar–CO₂ molecule. The accuracy of the PESs was validated
8 by their agreement with the vibrational spectrum of the rare-gas
9 complexes. The intermolecular and intramolecular vibrational excitation
10 energies were computed at the vibrational self-consistent field and
11 vibrational configuration interaction levels of theory. Overall, the
12 agreement between theory and experiment is excellent throughout the
13 vibrational spectra. The observed slight splitting of the bending modes,
14 resulting from their nondegeneracy in the complexes, is confirmed by
15 our computations, and the results qualitatively agree with the
16 experiment. The splitting increases with increasing polarizability of the
17 rare-gas atom. Additionally, we explain a discrepancy in the mode assignment in the intermolecular region of the neon complex with
18 our VCI character assignment.



1. INTRODUCTION

19 Carbon dioxide and its van der Waals complexes play a pivotal
20 role in atmospheric and environmental chemistry, leading to
21 extensive experimental and theoretical studies. This widespread
22 interest in the role of CO₂ naturally extends to its interactions
23 in van der Waals complexes, such as argon–carbon dioxide
24 (Ar–CO₂), neon–carbon dioxide (Ne–CO₂), and krypton–
25 carbon dioxide (Kr–CO₂), where unique weak intermolecular
26 interactions emerge. These interactions lead to minimum
27 energy structures in the classic C_{2v} T-shaped configuration,
28 which has been observed experimentally for each of the
29 complexes.¹ Additionally, vibrational spectroscopy, especially
30 infrared spectroscopy, has been an invaluable tool in probing
31 these subtle interactions through the investigation of the
32 potential energy surface (PES) and dynamics of the chemical
33 complexes. Understanding these molecular interactions is not
34 just of academic interest but also pivotal in comprehending the
35 importance of carbon dioxide in climate phenomena like the
36 greenhouse effect.

37 Utilizing vibrational spectroscopy, our study delves into the
38 detailed vibrational structure of the Ne–CO₂ and Kr–CO₂
39 complexes, which exhibit nuanced differences from the isolated
40 carbon dioxide molecule. Investigations of the rare-gas carbon
41 dioxide complexes mostly emphasize van der Waals inter-
42 actions, specifically the two fundamental vibrations in the
43 intermolecular region: the bending mode and the stretching
44 mode. For the neon complex, these frequencies have been
45 observed at 17.9 and 38.6 cm⁻¹, respectively.² For krypton, the
46 van der Waals bend and stretch energy levels were reported at

29.4 and 34.4 cm⁻¹, respectively.^{2–4} Similarly, recent⁴⁷ theoretical studies align with these experimental findings.⁵ Importantly, the intramolecular frequency shifts within these⁴⁸ complexes have been a focus of exploration. The splitting of⁴⁹ the degenerate intramolecular bending modes was shown⁵⁰ experimentally for the rare-gas complexes. This splitting⁵¹ appears to increase with increasing polarizability of the⁵² molecule, and the in-plane bend was consistently found to⁵³ be lower in energy than the out-of-plane bend. Specifically, for⁵⁴ the Ne–CO₂ complex, the splitting was determined to be⁵⁵ approximately 0.2 cm⁻¹, and for the Kr–CO₂ complex, the⁵⁶ splitting was observed to be about 1.5 cm⁻¹. Previously for the⁵⁷ Ar–CO₂ complex, we found a similar splitting of the bending⁵⁸ modes to be quite close to the experimental results of 0.8 cm⁻¹.⁶ Lastly, Fermi resonance can be observed experimentally⁵⁹ for each rare-gas carbon dioxide complex contributing to a⁶⁰ comprehensive understanding of the vibrational dynamics in⁶¹ noble gas–carbon dioxide complexes.⁶²

To achieve accurate vibrational structure predictions, a⁶³ precise PES is essential. Previously, permutationally invariant⁶⁴ polynomials have been developed and implemented to⁶⁵

Received: January 30, 2024

Revised: April 4, 2024

Accepted: April 15, 2024

Table 1. Fitting Accuracy for the Rg–CO₂ Two-Body Energy Function^a

		configs.	RMSE	RMSE low	χ^2	MAX	MAX low
Ne	training set	41,354	0.8488	4.998×10^{-6}	3.3543	69.330	0.01507
	test set	10,234	0.8088	1.280×10^{-6}		69.545	0.01511
Kr	training set	41,833	2.8785	6.968×10^{-5}	35.681	78.288	0.07903
	test set	10,358	2.8093	1.751×10^{-5}		73.188	0.04008

^aThe root-mean-squared error (RMSE), mean absolute error, and maximum errors are shown over the entire training and test set and for the low-energy configurations of each in units of kcal mol⁻¹. The χ^2 value has units of (kcal mol⁻¹)². The low parameters only include structures with energies within the ΔE range.

generate such surfaces.^{7–9} In our prior work, we utilized permutationally invariant polynomials fitted to electronic structure energies computed at the CCSD(T)-F12b level of theory with the aug-cc-pVTZ basis set to enable the development of a flexible-monomer two-body potential function for carbon dioxide argon dimer.⁶ A similar functional form was also established for both CO₂ monomers and dimers.¹⁰ The accuracy of these potential energy functions (PEFs) was validated through vibrational structure computations for the CO₂ monomer, dimer, and trimer, as well as Ar–CO₂ dimer.⁶ Our predicted data exhibited excellent agreement with experimental band assignments and energy levels for each molecular system. Notably, our model demonstrated remarkable precision in predicting the Fermi dyad peaks in the intramolecular region, the mode–mode coupling of the vibrations in the low-frequency intermolecular region, and the splitting of bending modes in the Ar–CO₂ complex.⁶ Furthermore, our model successfully assigned vibrational frequencies that were previously poorly characterized experimentally, as was the case for the cyclic trimer.

The accuracy of the theoretical vibrational energy levels is governed by the choice of the vibrational structure approach. Typically, a hierarchy of vibrational structure methods—including the harmonic approximation, vibrational self-consistent field (VSCF) theory, and vibrational configuration interaction (VCI) theory—is applied to ensure the convergence of the vibrational energy levels by more rigorously solving the vibrational Hamiltonian.¹¹ Combined, an accurate PEF and hierarchical vibrational structure methods can be used to simulate the vibrational spectrum of the chemical system with accuracy compared to the experiment. In this article, we develop two new flexible-monomer two-body PESs using a model function constructed from permutationally invariant polynomials. These functions are trained on ab initio reference energies of the Ne–CO₂ and Kr–CO₂ complexes. We then employ the PEFs into the vibrational Hamiltonian and determine vibrational energy levels solved at the VSCF and VCI levels of theory.

2. COMPUTATIONAL DETAILS

2.1. Potential Energy Surface. Previously, we developed a PEF of CO₂–Ar using permutationally invariant polynomials fit to the electronic energies of the carbon dioxide monomer and the argon–carbon dioxide dimer.⁶ Currently, we extend this approach to investigate the rare-gas–carbon dioxide complexes of neon and krypton. The intramolecular degrees of freedom of the carbon dioxide molecule were modeled by a one-body PEF fit to over 170,000 configurations of CO₂ monomers computed at the CCSD(T)-F12b level of theory with the aug-cc-pVTZ basis set using a sixth-degree symmetrized polynomial function. For further details on the one-body PEF and the training set used to generate it, readers

are encouraged to consult our prior publication.¹⁰ In the current work, we develop the two-body PEF for the Rg–CO₂ dimers by using a fifth-degree polynomial function consisting of intramolecular and intermolecular exponential functions for each of the six interatomic distances in each complex. These two-body PEFs are built from a linear combination of unique symmetrized polynomials, which not only account for the intermolecular dynamics in the Rg–CO₂ complex but also for the intramolecular degrees of freedom of the CO₂ molecule. The entire model function can be found in the authors' GitHub repository.

For each rare-gas complex, a training set of at least 41,000 unique configurations was computed at the CCSD(T)-F12b/aug-cc-pVTZ level of theory and basis set with the Molpro software package.¹² The training set was generated through projections along the fundamental and combination vibrational modes. Both the intermolecular and intramolecular degrees of freedom were considered for each molecule at the global minimum energy (T-shaped) structure and transition-state (linear) structure. Additional configurations were generated using a three-dimensional grid, whose coordinates included the intermolecular stretch distance, the intermolecular bend angle, and the intramolecular symmetric stretch of each molecule. In this way, configurations further from the energy minimums were explored. Lastly, configurations where the atomic coordinates were randomly perturbed were also incorporated into each training set. These can be found in the authors' GitHub repository.

The training sets were used to fit the flexible-monomer two-body PEF. Linear and nonlinear coefficients were optimized via Tikhonov regularization,¹³ minimizing the weighted sum of the squared errors according to the following equation

$$\chi^2 = \sum_n w_n [V^{\text{model}}(n) - V^{\text{ref}}(n)]^2 + \Gamma \sum_k c_k^2 \quad (1)$$

Here, k runs over the list of linear coefficients, n runs over the list of training set configurations, and Γ represents the regularization term, set to 5.0×10^{-2} , which mitigates overfitting. The model and reference energies for the n th configuration are given as $V^{\text{model}}(n)$ and $V^{\text{ref}}(n)$, respectively. The weighting factor (w_n), which stresses configurations with lower total energies, is expressed as

$$w(E) = \left(\frac{\Delta E}{E - E_{\min} + \Delta E} \right)^2 \quad (2)$$

where E_{\min} is the minimum energy value and ΔE , set to 10 kcal mol⁻¹, is the energy range for selecting the subset of emphasized configurations.

The fits of each model potential with respect to the reference energies, as shown in Table 1, are very accurate, especially in the low-energy range. Here, the largest deviation

165 from the test set energies was 0.01511 and 0.04008 kcal mol⁻¹
 166 for Ne and Kr, respectively. More than 10,000 configurations
 167 were used for the test set for each model potential, and
 168 notably, the root-mean-squared error (RMSE) and maximum
 169 error were comparable in the training and the test sets.

170 **2.2. Vibrational Schrödinger Equation.** The rare-gas–
 171 carbon dioxide complex PESs are included in a vibrational
 172 Hamiltonian with general curvilinear coordinates. This
 173 Hamiltonian is separable and can be decomposed into its
 174 kinetic energy and potential energy terms.^{14,15} In this article,
 175 we employ the notation introduced by Strobusch and
 176 Scheurer^{14,15} to refer to the many-body expansion orders for
 177 Hamiltonian terms, as $V(O_V)/T(O_M, O_K, O_{VG}, O_{Vg})$. These
 178 components refer to the potential energy term (V), on-
 179 diagonal (M) and off-diagonal (K) elements of the kinetic
 180 energy operator G matrix terms, the ∇G term, and the
 181 pseudopotential term, commonly denoted as V_g . For the Rg–
 182 CO₂ complexes, we employ a reduced-dimensional vibrational
 183 Hamiltonian, $V(3)/T(3,3,3,3)$. We previously reported the
 184 convergence of vibrational frequencies using the VSCF
 185 approach compared to the full expansion, $V(6)/T(6,6,6,6)$,
 186 for the Ar–CO₂.⁶

187 We employ the VSCF^{16–19} and the VCI approaches^{20–22} to
 188 solve the vibrational Schrödinger equation. The harmonic
 189 approximation solutions are also reported within the NITRO-
 190 GEN software package.²³ The VSCF approach is exact only
 191 when the Hamiltonian is additively separable and defines
 192 solutions to the Schrödinger equation wave functions as
 193 products of one-mode functions. The VCI calculations
 194 explicitly consider mode–mode interactions, which can be
 195 quantified by analyzing the wave function contributions. In this
 196 work, only configurations with a maximum sum of VCI quanta
 197 less than 15 (a total of 38,760 VSCF configurations) were
 198 considered. At this level, the vibrational frequencies are well
 199 converged. All excited state energies and VCI configuration
 200 amplitudes can be found in the authors' GitHub repository
 201 (<http://github.com/sodelab>).

3. RESULTS AND DISCUSSION

202 **3.1. Structural Parameters.** The ground-state global
 203 minimum energy structure of each Rg–CO₂ complex was
 204 found to be T-shaped ($\theta = 90.0^\circ$), as shown in Table 2. The

Table 2. Structural Parameters of the Ground-State Minimum of the Ne–CO₂, Ar–CO₂, and Kr–CO₂ Complexes^a

		R	θ	r_{CO}	energy
Ne	Chen et al. ²⁴	3.15	90.0		-93.05
	this work	3.150	90.0	1.1622	-89.02
	experiment ¹	3.2904	81.42		
Ar	Cui et al. ²⁵	3.440	90.0		-200.97
	Zhao et al. ²⁶	3.432	90.0		-199.38
	previous work	3.436	90.0	1.1622	-195.96
Kr	Chen et al. ⁵	3.5039	83.10		
	this work	3.596	90.0	1.1622	-231.70
	experiment ¹	3.6243	83.28		-213.34

^aThe intermolecular distance between the Rg and CO₂, R , and the average intramolecular CO₂ distance between C and O atoms, r_{CO} , are reported in angstroms. The angle θ is reported in degrees. The well depth is reported in cm⁻¹.

205 intermolecular distance, R , for the neon complex was found to 205
 206 be 3.150 Å at the global minimum, and for the krypton 206
 207 complex, R was determined as 3.596 Å. Previously for the for 207
 208 Ar–CO₂ complex, the minimum energy intermolecular 208
 209 distance was found between these two values.⁶ Additionally, 209
 210 our optimized structural parameters agree quite well with the 210
 211 experiment. For the neon complex, the experiment shows this 211
 212 intermolecular distance at 3.2904 Å, and for krypton complex, 212
 213 the distance is 3.6243 Å.¹ The angles are slightly less than 213
 214 90.0° in both the neon and krypton complexes—81.42 and 214
 215 83.28°, respectively. As is noted in previous studies, the 215
 216 computed parameters reflect the equilibrium structure of each 216
 217 Rg–CO₂ complex, whereas the experimental values represent 217
 218 the zero-point energy structure. We also show good agreement 218
 219 with respect to the other theoretical studies.^{5,24–26} We also 219
 220 present the well depths for the neon and krypton complexes, 220
 221 which are -89.02 and -213.34 cm⁻¹, respectively. Notably, 221
 222 our PES is capable of treating the intramolecular carbon– 222
 223 oxygen distance of the complexes, and in each case, the 223
 224 minimum energy structure is found to have a intramolecular 224
 225 distance (r_{CO}) equal to 1.1622 Å.²²⁵

226 A local energy-minimum linear structure is found for each 226
 227 complex, similar to the argon complex. Notably, no experiment 227
 228 has found the stable linear structure. Here, the intermolecular 228
 229 distances in the neon and krypton complexes are found to be 229
 230 4.304 and 4.770 Å, respectively, and the well depths for these 230
 231 compounds are -55.22 and -124.25 cm⁻¹, respectively. The 231
 232 intramolecular r_{CO} bonds remain unchanged for the neon 232
 233 complex (1.1622 Å) but are slightly larger on average in the 233
 234 case of krypton (1.1623 Å). For comparison, our previous Ar– 234
 235 CO₂ linear complex results indicate a carbon–argon distance 235
 236 of 4.620 Å, an intramolecular r_{CO} bond distance of 1.1623, and 236
 237 a well depth of -115.42 cm⁻¹.⁶

238 **3.2. Neon Intermolecular Vibrational Frequency**
 239 **Region.** We present the first five intermolecular vibrations 239
 240 for the T-shaped Ne–CO₂ complex in Table 3. We employ 240 t3

Table 3. Intermolecular Vibrational Energy Levels (in cm⁻¹) of the Ne–CO₂ Complex Obtained with the Harmonic Approximation, VSCF, and VCI Methods Are Compared to Experimental and Theoretical Values from the Literature

	HAR	VSCF	VCI	expt. ^{1,2,27}	Chen et al. ²⁴
ν_b	25.37	19.84	17.76	17.9, 17.716	17.94
ν_s	39.69	28.48	23.91	38.6	23.19
$2\nu_b$		36.89	36.22		
$\nu_b + \nu_s$		45.35	37.58		
$2\nu_s$		49.33	44.18		

241 three levels of increasingly accurate vibrational structure 241
 242 methods (i.e., the harmonic approximation, VSCF and VCI) 242
 243 and present the results alongside experimental and theoretical 243
 244 values from the literature. Two fundamental modes exist in this 244
 245 region: the intermolecular bend (ν_b) and the intermolecular 245
 246 stretch (ν_s). At each level of theory, the bend mode is found to 246
 247 have a lower excitation energy than the stretch mode, which 247
 248 corresponds to what was shown previously for the Ar–CO₂ 248
 249 complex.⁶ At the VCI level, the bend frequency is found to be 249
 250 17.76 cm⁻¹, compared to 17.9 and 17.716 cm⁻¹, experimen- 250
 251 tally.^{1,2,27} This agreement shows the accuracy of the vibrational 251
 252 approximation and the PES. The stretch frequency is found at 252
 253 23.91 cm⁻¹ at the VCI level and, similar to the bend mode, 253
 254 relaxes at higher levels of theory. Chen et al. report theoretical 254

255 intermolecular bend and stretch excitation energies at 17.94
 256 and 23.19 cm^{-1} , respectively, which match exceptionally well
 257 with our computed results. Interestingly, both theoretical
 258 results for the stretch frequency disagree with the exper-
 259 imentally determined value previously reported. We will
 260 address this disagreement by looking at the combination
 261 bands in the intermolecular region and by re-emphasizing that
 262 the experimentally determined vibrational excitation energies
 263 in this region are obtained through combination bands in the
 264 CO_2 intramolecular asymmetric stretching region. These
 265 intramolecular and intermolecular combination modes will
 266 be explored in the following section.

267 Additionally, we report three overtone and combination
 268 vibrational frequencies in this region of the complex in **Table 3**.
 269 At the VCI level, we see the intermolecular bend overtone
 270 ($2\nu_b$), the bend and stretch combination ($\nu_b + \nu_s$), and the
 271 intermolecular stretch overtone ($2\nu_s$) at 36.22, 37.58, and
 272 44.18 cm^{-1} , respectively. Interestingly, the coefficients of the
 273 VCI wave function for the bending overtone point toward the
 274 explanation for the assignment discrepancy between the
 275 experiment and theory.

$$276 \Psi_{2\nu_b}^{\text{VCI}} = 0.596 \Psi_{\nu_s}^{\text{VSCF}} + 0.522 \Psi_{2\nu_b}^{\text{VSCF}} + \dots \quad (3)$$

277 The leading VSCF mode contribution to the mode we have
 278 labeled as the intermolecular bend overtone ($2\nu_b$) is in fact the
 279 van der Waals stretch fundamental ($\Psi_{\nu_s}^{\text{VSCF}}$). Thus, it might
 280 make more sense to label this mode as another van der Waals
 281 stretch. It should also be noted that the van der Waals stretch
 282 frequency at 23.91 cm^{-1} ($\Psi_{\nu_s}^{\text{VCI}}$) also has intermolecular bend
 283 overtone character but to a lesser degree. This combined
 284 character makes simple assignment of the modes in this region
 285 difficult. However, it also helps explain why we see the
 286 experimental assignment of the intermolecular stretch around
 287 38 cm^{-1} since this peak does in fact contain van der Waals
 288 stretch character. Vibrational mode assignment in the complex
 289 will be explored in detail further in the intramolecular region,
 290 in particular as it relates to Fermi resonance and the
 291 intramolecular bending mode splitting.

292 **3.3. Neon Intramolecular Vibrational Frequency**
 293 **Region.** The intramolecular frequencies of the $\text{Ne}-\text{CO}_2$
 294 complex are shown in **Table 4**. The first eight frequencies
 295 correspond to the intramolecular vibrations of the CO_2 in the
 296 van der Waals complex, four of which are fundamental
 297 vibrations: in-plane and out-of-plane intramolecular bends (ν_2^i
 298 and ν_2^o , respectively), symmetric stretch (ν_1), and the
 299 asymmetric stretch (ν_3). Additionally, we report combination,
 300 overtone, and Fermi dyad bands arising from these intra-
 301 molecular CO_2 vibrations, as well as combinations of the
 302 asymmetric stretch intramolecular mode and the intermolec-
 303 ular mode vibrations. These latter values may provide
 304 additional insights into the frequencies from **Table 3**, especially
 305 regarding the experiment.

306 The two in-plane and out-of-plane intramolecular bending
 307 modes in the $\text{Ne}-\text{CO}_2$ complex, as shown in **Table 4**, are
 308 observed to have frequencies of 668.47 and 668.73 cm^{-1} ,
 309 respectively, at the VCI level of theory. We found previously
 310 the degenerate bending modes of the isolated CO_2 molecule at
 311 667.8 cm^{-1} at the same level of theory,²⁹ compared to 667.380
 312 cm^{-1} experimentally.³⁰ The observed nondegeneracy at all
 313 levels of theory for the intramolecular bending modes is also
 314 consistently observed in the $\text{Ar}-\text{CO}_2$ complex. However, for
 315 the current $\text{Ne}-\text{CO}_2$ complex, the magnitude of the symmetry

Table 4. Intramolecular Vibrational Energy Levels (in cm^{-1}) of the $\text{Ne}-\text{CO}_2$ Complex Obtained with the Harmonic Approximation, VSCF, and VCI Methods^a

	HAR	VSCF	VCI	expt. ^{1,3,27,28}
ν_2^i	673.18	670.46	668.47	667.380
ν_2^o	673.36	670.69	668.73	667.436
$2\nu_2^o/2\nu_2^i$			1285.53 ^b	
$2\nu_2^i$		1341.08	1338.73	
$2\nu_2^o$		1341.25	1338.73	
$\nu_2^o + \nu_2^i$		1343.01	1338.71	
ν_1	1352.54	1349.54	1389.32 ^b	
ν_3	2394.59	2353.59	2348.37	2349.280
$\nu_3 + \nu_b$		2373.31	2366.05	2366.9960
$\nu_3 + \nu_s$		2382.02	2372.55	
$\nu_3 + 2\nu_b$		2390.26	2385.28	
$\nu_3 + \nu_b + \nu_s$		2398.81	2386.6	
$\nu_3 + 2\nu_s$		2402.86	2393.09	
$\nu_3 + \nu_2^i$		3011.79	3004.57	3004.154
$\nu_3 + \nu_2^o$		3012.02	3004.84	3004.204
$2\nu_2^o/2\nu_2^i + \nu_3$		3670.33	3612.74 ^b	3612.98919
$\nu_1 + \nu_3$		3698.98	3715.76 ^b	3714.97590

^aNote that unlike in the isolated CO_2 monomer, the bending modes, ν_2^o and ν_2^i , are no longer degenerate. ^bThe Fermi dyad bands are denoted with an asterisk.

breaking of the degenerate bend modes is about 0.2 cm^{-1} with the in-plane bend being consistently less energetic than the out-of-plane bend. This agrees with recent experimental observation showing the in-plane bend 0.057 cm^{-1} lower in energy than the out-of-plane bend. The experimental bending frequency values in **Table 4** are obtained by adding this difference to the energy level of the experimentally determined isolated monomer bending mode.²⁷

The remaining fundamental frequencies in this region remain mostly unchanged from the isolated CO_2 monomer. We compute the asymmetric stretch vibrational excitation in the complex as 2348.37 cm^{-1} , at the VCI level, compared to 2349.28 cm^{-1} , experimentally.^{1,27} For comparison, the isolated ν_3 band in the isolated CO_2 molecule is detected at 2349.2 cm^{-1} .³⁰ Our theoretical results for the asymmetric stretch frequency in the complex are shown to be about one wavenumber lower in energy than the experiment. This trend was observed for the $\text{Ar}-\text{CO}_2$ molecule previously and holds also for the $\text{Kr}-\text{CO}_2$ molecule. In the symmetric stretch region, the fundamental frequency for the complex is found at 1349.54 cm^{-1} , compared to 1340.4 cm^{-1} in the isolated molecule, at the VSCF level. There is no direct comparison to the experiment (or VCI) due to its large mode mixing, characteristically known as Fermi resonance. In general, the agreement underscores the accuracy of our method across different molecular systems.

The Fermi dyad peaks found in the symmetric stretch region, denoted as $2\nu_2^o/2\nu_2^i$ and ν_1 , are detected at 1285.53 and 1389.32 cm^{-1} , at the VCI level. This indicates a very weak perturbation from the isolated monomer potential with Fermi dyad peaks observed at 1284.7 and 1388.7 cm^{-1} . The Fermi mixed $2\nu_2^o/2\nu_2^i + \nu_3$ and $\nu_1 + \nu_3$ modes are observed experimentally at 3612.99 and 3714.98 cm^{-1} , which agrees quantitatively with our VCI frequencies of 3612.74 and 3715.76 cm^{-1} , respectively.³

Due to the complete PES treatment of the $\text{Ne}-\text{CO}_2$ complex in the vibrational Schrodinger equation, we can

evaluate the combination bands between intermolecular and intramolecular interactions in the asymmetric stretching region and compare these values to the intermolecular mode frequencies in Table 4. The ordering for the combination modes follows that of the intermolecular modes: ν_b , ν_s , $2\nu_b$, $\nu_b + \nu_s$, and $2\nu_s$. The largest deviation in energy amounts to about 0.7 cm^{-1} , which further justifies the reduced dimensional treatment.

3.4. Krypton Intermolecular Vibrational Frequency

Region. The first five intermolecular vibrations for the T-shaped Kr–CO₂ complex are shown in Table 5. As with the

Table 5. Intermolecular Vibrational Energy Levels (in cm^{-1}) of the Kr–CO₂ Complex Obtained with the Harmonic Approximation, VSCF, and VCI Methods Are Compared to Experimental and Theoretical Values from the Literature

	HAR	VSCF	VCI	expt. ^{2–4}	Chen et al. ⁵
ν_b	32.00	29.25	27.60	31.6, 29.429	30.027
ν_s	35.98	32.74	30.37	34.4, 42.4	32.233
$2\nu_b$		55.7	52.79		
$\nu_b + \nu_s$		61.1	53.20		
$2\nu_s$		62.18	58.53		

neon complex, we report the vibrational excitation energies at the harmonic approximation, VSCF, and VCI levels theory alongside experimental and theoretical values from the literature. Again, the van der Waals bend fundamental is consistently lower in energy than the van der Waals stretch frequency at all levels of theory. At the VCI level, the difference between the bend and stretch frequencies is 2.77 cm^{-1} . This matches with the differences observed experimentally of 2.80 and $>2.5 \text{ cm}^{-1}$,^{2,4} however, our computed results are shifted lower in energy by about 2 cm^{-1} compared to the experiment. Chen et al. report the two fundamental intermolecular frequencies at 30.027 and 32.233 cm^{-1} for the bend and stretch, respectively.⁵ Conversely, the empirically determined stretch frequency found at 42.4 cm^{-1} seems to be an outlier compared to the other computed and detected values.³

We report the combination and overtone frequencies for this region, as well, and observe the same ordering as the neon complex: the bending overtone, the stretch and bend combination, and the stretch overtone. The VCI level of theory relaxes the computed VSCF excitation energies as they are observed at 52.79, 53.20, and 58.53 cm^{-1} , respectively. To our knowledge, no direct experimental observations have been made for these frequencies. Next, we will explore in detail the vibrational frequencies in the intramolecular region.

3.5. Krypton Intramolecular Vibrational Frequency

Region. The intramolecular vibrational frequencies for the Kr–CO₂ complex are reported in Table 6. Again, the four CO₂ fundamental vibrations (in-plane and out-of-plane intramolecular bends, symmetric stretch, and the asymmetric stretch) are shown, alongside the other intramolecular modes, including the Fermi dyad and other combination bands involving the intermolecular motions of the complex.

In the intramolecular bend region of the vibrational spectrum, we observe the same relative ordering of the in-plane and out-of-plane vibrations compared to the other rare-gas complexes: the in-plane bend found at 666.68 cm^{-1} is less energetic than the out-of-plane bend observed at 668.58 cm^{-1} . However, the splitting here is much larger than that for the other molecules. Table 7 shows the experimental and

Table 6. Intramolecular Vibrational Energy Levels (in cm^{-1}) of the Kr–CO₂ Complex Obtained via Harmonic Approximation, VSCF, and VCI Methods

	HAR	VSCF	VCI	expt. ^{1,3,4,28}
ν_2^i	670.68	668.60	666.58	667.380
ν_2^o	672.98	670.36	668.53	668.798
$2\nu_2^o/2\nu_2^i$			1284.39 ^a	
$2\nu_2^i$		1337.41	1336.46	
$\nu_2^o + \nu_2^i$		1340.62	1336.48	
$2\nu_2^o$		1340.64	1336.46	
ν_1	1352.09	1349.22	1284.39 ^a	
ν_3	2393.40	2352.59	2347.39	2348.259205
$\nu_3 + \nu_b$		2381.99	2375.09	
$\nu_3 + \nu_s$		2385.38	2377.84	
$\nu_3 + 2\nu_b$		2408.59	2400.69	
$\nu_3 + \nu_b + \nu_s$		2413.85	2401.19	
$\nu_3 + 2\nu_s$		2414.87	2406.09	
$2\nu_2^o/2\nu_2^i + \nu_3$		3668.74	1284.39 ^a	3610.86796
$\nu_1 + \nu_3$		3697.68	1284.39 ^a	3713.02414

^aThe Fermi dyad bands are denoted with an asterisk.

Table 7. Experimental and Theoretical CO₂ ν_2 Splitting Values for the Rare-Gas Dimers in cm^{-1} ^a

	VCI	expt.
Ne–CO ₂	0.26	0.057
Ar–CO ₂ ⁶	0.83	0.877
Kr–CO ₂	1.95	1.418

^aFor each complex, the out-of-plane bend was observed as more energetic than the in-plane bend. The theoretical values are shown at the VCI level of theory.

theoretical CO₂ ν_2 splitting values for the neon, argon, and krypton complexes.⁶ For Kr–CO₂, we compute a splitting of 1.95 cm^{-1} compared to the 1.418 cm^{-1} experimentally determined value.⁴

In the symmetric stretch region, the upper and lower Fermi dyad peaks (denoted again as $2\nu_2^o/2\nu_2^i$ and ν_1) are found at 1284.39 and 1388.21 cm^{-1} , respectively. Again, this represents a weak perturbation from the isolated monomer. Unfortunately, no experimental data exist for these assignments; however, the Fermi dyad that results from a combination band with the asymmetric mode frequency is observed. The experimental lower and upper peaks are found at 3610.87 and 3713.02 cm^{-1} , respectively, compared to our VCI frequencies at 3610.54 and 3713.67, respectively.³ This near perfect agreement points toward the accuracy of the lower peaks.

The asymmetric stretch frequency for the complex was found at 2347.39 cm^{-1} at the VCI level, again about 1 cm^{-1} below the experimental peak.¹ In this region as well, the intermolecular combination bands were also found in the same ordering as before: ν_b , ν_s , $2\nu_b$, $\nu_b + \nu_s$, and $2\nu_s$. The difference between these combination bands and the asymmetric stretch frequency results in frequencies that closely match the intermolecular vibrational excitations before. The largest deviation in energy amounts to about 0.6 cm^{-1} , again justifying the reduced dimensional treatment.

4. CONCLUSIONS

Extending on our work in the Ar–CO₂ system, we have developed two new flexible-monomer two-body PEFs for the

431 Ne–CO₂ and Kr–CO₂ systems fit to energies at the
432 CCSD(T)-F12b/aug-cc-pVTZ level of theory. In both
433 molecules, as is the case for the argon complex, both the T-
434 shaped global minimum and linear local minimum were found.
435 The vibrational structure of both T-shaped complexes was
436 explored using the harmonic approximation and VSCF, as well
437 as the experimentally accurate VCI approach. The vibrational
438 frequencies in the intermolecular and intramolecular regions
439 were presented and compared quite accurately to experiment
440 and previous theoretical results. In particular, for the Ne–CO₂
441 complex, our work was able to clarify the previous discrepancy
442 between the theoretical and experimental frequency for the
443 intermolecular stretch. The experimental band peak is most
444 likely associated with a mixed vibrational motion that contains
445 van der Waals bend overtone and van der Waals stretch
446 character. This peak found at 38.6 cm^{−1} experimentally
447 matches well with our peak at 36.22 cm^{−1}. In the intra-
448 molecular bending region for both molecules, the experimental
449 trend for the splitting of the bending modes is observed. We
450 report the out-of-plane bend frequency to be 0.26 and 1.95
451 cm^{−1} more energetic than the in-plane bend frequency for the
452 neon and krypton complexes, respectively. The computed
453 Fermi resonance peaks quantitatively agreed with the experi-
454 ment in both complexes to within 1 cm^{−1} in the asymmetric
455 stretch and symmetric stretch combination band region.
456 Future work will explore the helium and xenon systems, and
457 it is presently underway.

458 ■ ASSOCIATED CONTENT

459 Data Availability Statement

460 Furthermore, the PES and training set data are openly available
461 in the authors' GitHub repository ([https://github.com/
462 sodelab](https://github.com/sodelab)).

463 ■ Supporting Information

464 The Supporting Information is available free of charge at
465 <https://pubs.acs.org/doi/10.1021/acs.jpca.4c00639>.

466 Breakdown of the VCI mode contributions in the
467 intramolecular and intermolecular regions of both
468 complexes as well as the optimized geometries (ZIP)

469 Ne–CO₂ intermolecular contributions, neon intra-
470 molecular mode-mixing contributions, and Kr–CO₂
471 intermolecular and intermolecular mode–mode contrib-
472 utions (PDF)

473 ■ AUTHOR INFORMATION

474 Corresponding Author

475 Olaseni Sode – Department of Chemistry and Biochemistry,
476 California State University, Los Angeles, Los Angeles,
477 California 90032, United States;  [orcid.org/0000-0002-
478 5236-8670](https://orcid.org/0000-0002-5236-8670); Email: osode@calstatela.edu

479 Authors

480 Larry Rodriguez – Department of Chemistry and
481 Biochemistry, California State University, Los Angeles, Los
482 Angeles, California 90032, United States;  [orcid.org/
483 0000-0002-2527-7204](https://orcid.org/0000-0002-2527-7204)

484 Michael Natalizio – Department of Chemistry and
485 Biochemistry, California State University, Los Angeles, Los
486 Angeles, California 90032, United States

487 Complete contact information is available at:
488 <https://pubs.acs.org/10.1021/acs.jpca.4c00639>

Notes

The authors declare no competing financial interest.

■ ACKNOWLEDGMENTS

This research was supported by the American Chemical Society Petroleum Research Fund (grant no. S8240-UN16) and the National Science Foundation Partnerships for Research and Education in Chemistry (PREC) Program (grant no. CHE-2216858). Computing resources were provided by ACCESS (TG-CHE170085). L.R. was supported by the National Institute of General Medical Sciences of the National Institute of Health (grant no. 5T32GM146700-02) and the PREC Program of the National Science Foundation (grant no. CHE-2216858).

■ REFERENCES

- (1) Randall, R. W.; Walsh, M. A.; Howard, B. J. Infrared absorption spectroscopy of rare-gas – CO₂ clusters produced in supersonic expansions. *Faraday Discuss. Chem. Soc.* **1988**, *85*, 13–21.
- (2) Iida, M.; Ohshima, Y.; Endo, Y. Induced dipole moments and intermolecular force fields of rare gas–carbon dioxide complexes studied by Fourier-transform microwave spectroscopy. *J. Phys. Chem.* **1993**, *97*, 357–362.
- (3) Fraser, G. T.; Pine, A. S.; Suenram, R. D. Optothermal-infrared and pulsed-nozzle Fourier-transform microwave spectroscopy of rare gas–CO₂ complexes. *J. Chem. Phys.* **1988**, *88*, 6157–6167.
- (4) Gartner, T.; Ghebretnsae, S.; McKellar, A. R. W.; Moazzeni, N. Spectra of CO₂–Kr in the 4.3 μ m region: Intermolecular Bend and Symmetry Breaking of the Intramolecular CO₂ Bend. *ChemistrySelect* **2022**, *7*, No. e202202601.
- (5) Chen, R.; Zhu, H.; Xie, D. Intermolecular potential energy surface, microwave and infrared spectra of the Kr–CO₂ complex from ab initio calculations. *Chem. Phys. Lett.* **2011**, *511*, 229–234.
- (6) Sode, O.; Ruiz, J.; Peralta, S. Theoretical investigation of the vibrational structure of the Ar–CO₂ complex. *J. Mol. Spectrosc.* **2021**, *380*, 111512.
- (7) Braams, B. J.; Bowman, J. M. Permutationally invariant potential energy surfaces in high dimensionality. *Int. Rev. Phys. Chem.* **2009**, *28*, 524 577–606.
- (8) Xie, Z.; Bowman, J. M. Permutationally invariant polynomial basis for molecular energy surface fitting via monomial symmetrization. *J. Chem. Theory Comput.* **2010**, *6*, 26–34.
- (9) Wang, Q. K.; Bowman, J. M. Two-component, *ab initio* potential energy surface for CO₂–H₂O, extension to the hydrate clathrate, CO₂–(H₂O)₂₀, and VSCF/VCI vibrational analyses of both. *J. Chem. Phys.* **2017**, *147*, 161714.
- (10) Sode, O.; Cherry, J. N. Development of a Flexible-Monomer Two-Body Carbon Dioxide Potential and Its Application to Clusters up to (CO₂)₁₃. *J. Comput. Chem.* **2017**, *38*, 2763–2774.
- (11) Christiansen, O. Vibrational structure theory: new vibrational wave function methods for calculation of anharmonic vibrational energies and vibrational contributions to molecular properties. *Phys. Chem. Chem. Phys.* **2007**, *9*, 2942–2953.
- (12) Werner, H.-J.; Knowles, P. J.; Knizia, G.; Manby, F. R.; Schütz, M. Molpro: a general-purpose quantum chemistry program package. *Wiley Interdiscip. Rev. Comput. Mol. Sci.* **2012**, *2*, 242–253.
- (13) Tikhonov, A. N.; Goncharsky, A.; Yagola, A. G. *Numerical Methods for the Solution of Ill-Posed Problems*; Springer: Netherlands, 1995.
- (14) Strobusch, D.; Scheurer, C. Hierarchical expansion of the kinetic energy operator in curvilinear coordinates for the vibrational self-consistent field method. *J. Chem. Phys.* **2011**, *135*, 124102.
- (15) Strobusch, D.; Scheurer, C. The hierarchical expansion of the kinetic energy operator in curvilinear coordinates extended to the vibrational configuration interaction method. *J. Chem. Phys.* **2011**, *135*, 144101.

553 (16) Bowman, J. M. Self-consistent field energies and wavefunctions
554 for coupled oscillators. *J. Chem. Phys.* **1978**, *68*, 608–610.

555 (17) Gerber, R.; Ratner, M. A semiclassical self-consistent field (SC
556 SCF) approximation for eigenvalues of coupled-vibration systems.
557 *Chem. Phys. Lett.* **1979**, *68*, 195–198.

558 (18) Bowman, J. M. The self-consistent-field approach to polyatomic
559 vibrations. *Acc. Chem. Res.* **1986**, *19*, 202–208.

560 (19) Ratner, M. A.; Gerber, R. B. Excited vibrational states of
561 polyatomic molecules: the semiclassical self-consistent field approach.
562 *J. Phys. Chem.* **1986**, *90*, 20–30.

563 (20) Christoffel, K. M.; Bowman, J. M. Investigations of self-
564 consistent field, scf ci and virtual state-configuration interaction
565 vibrational energies for a model three-mode system. *Chem. Phys. Lett.*
566 **1982**, *85*, 220–224.

567 (21) Rauhut, G. Configuration selection as a route towards efficient
568 vibrational configuration interaction calculations. *J. Chem. Phys.* **2007**,
569 *127*, 184109.

570 (22) Scribano, Y.; Benoit, D. M. Iterative active-space selection for
571 vibrational configuration interaction calculations using a reduced-
572 coupling VSCF basis. *Chem. Phys. Lett.* **2008**, *458*, 384–387.

573 (23) Changala, P. B. NITROGEN, Numerical and Iterative Techniques
574 for Rovi-bronic Energies with General Internal Coordinates, 2018. <http://>
575 www.colorado.edu/nitrogen.

576 (24) Chen, R.; Jiao, E.; Zhu, H.; Xie, D. A new ab initio potential
577 energy surface and microwave and infrared spectra for the Ne–CO₂
578 complex. *J. Chem. Phys.* **2010**, *133*, 104302.

579 (25) Cui, Y.; Ran, H.; Xie, D. A new potential energy surface and
580 predicted infrared spectra of the Ar–CO₂ van der Waals complex. *J.*
581 *Chem. Phys.* **2009**, *130*, 224311.

582 (26) Zhao, A.; Shi, L.; Tian, Y.; Zheng, L.; Zheng, R. Theoretical
583 studies for the infrared spectra of Ar–CO₂ complex: Fundamental
584 and combination bands. *Spectrochim. Acta, Part A* **2018**, *204*, 308–
585 316.

586 (27) Barclay, A. J.; McKellar, A. R. W.; Moazzen-Ahmadi, N. New
587 infrared spectra of CO₂ – Ne: Fundamental for CO₂ – 22Ne
588 isotopologue, intermolecular bend, and symmetry breaking of the
589 intramolecular CO₂ bend. *Chem. Phys. Lett.* **2021**, *779*, 138874.

590 (28) Pine, A. S.; Fraser, G. T. Vibrational predissociation in the CO₂
591 dimer and trimer and rare gas–CO₂ complexes. *J. Chem. Phys.* **1988**,
592 *89*, 100–109.

593 (29) Maystrovsy, S.; Keçeli, M.; Sode, O. Understanding the
594 anharmonic vibrational structure of the carbon dioxide dimer. *J. Chem.*
595 *Phys.* **2019**, *150*, 144302.

596 (30) Chedin, A. The carbon dioxide molecule. *J. Mol. Spectrosc.*
597 **1979**, *76*, 430–491.